Atmos. Meas. Tech., 8, 171–182, 2015
www.atmos-meas-tech.net/8/171/2015/
doi:10.5194/amt-8-171-2015

Atmospheric Measurement Techniques
Open Access

Ionospheric assimilation of radio occultation and ground-based GPS data using non-stationary background model error covariance

C. Y. Lin[1], T. Matsuo[2,3], J. Y. Liu[1,4], C. H. Lin[5], H. F. Tsai[5], and E. A. Araujo-Pradere[2]

[1]Institute of Space Science, National Central University, Chungli, Taiwan
[2]Cooperative Institute for Research in Environmental Sciences, University of Colorado, Boulder, Colorado, USA
[3]Space Weather Prediction Center, National Oceanic and Atmospheric Administration, Boulder, Colorado, USA
[4]National Space Organization, HsinChu, Taiwan
[5]Department of Earth Sciences, National Cheng Kung University, Tainan, Taiwan

Correspondence to: J. Y. Liu (jyliu@jupiter.ss.ncu.edu.tw)

Received: 7 January 2014 – Published in Atmos. Meas. Tech. Discuss.: 14 March 2014
Revised: 3 December 2014 – Accepted: 3 December 2014 – Published: 12 January 2015

Abstract. Ionospheric data assimilation is a powerful approach to reconstruct the 3-D distribution of the ionospheric electron density from various types of observations. We present a data assimilation model for the ionosphere, based on the Gauss–Markov Kalman filter with the International Reference Ionosphere (IRI) as the background model, to assimilate two different types of slant total electron content (TEC) observations from ground-based GPS and space-based FORMOSAT-3/COSMIC (F3/C) radio occultation. Covariance models for the background model error and observational error play important roles in data assimilation. The objective of this study is to investigate impacts of stationary (location-independent) and non-stationary (location-dependent) classes of the background model error covariance on the quality of assimilation analyses. Location-dependent correlations are modeled using empirical orthogonal functions computed from an ensemble of the IRI outputs, while location-independent correlations are modeled using a Gaussian function. Observing system simulation experiments suggest that assimilation of slant TEC data facilitated by the location-dependent background model error covariance yields considerably higher quality assimilation analyses. Results from assimilation of real ground-based GPS and F3/C radio occultation observations over the continental United States are presented as TEC and electron density profiles. Validation with the Millstone Hill incoherent scatter radar data and comparison with the Abel inversion results are also presented. Our new ionospheric data assimilation model that employs the location-dependent background model error covariance outperforms the earlier assimilation model with the location-independent background model error covariance, and can reconstruct the 3-D ionospheric electron density distribution satisfactorily from both ground- and space-based GPS observations.

1 Introduction

The ionosphere is becoming more relevant to human society, with its reliance on modern technology, since the accuracy of navigation and quality of telecommunication is influenced by ionospheric conditions. Disruption of communications and navigation systems can have severe societal consequences. Even though the ionospheric observational techniques and the ionospheric models have gone through considerable development sustained over many decades, accurate monitoring and forecasting of the ionosphere conditions still presents obstinate challenges. Data assimilation procedures have recently come to play an important role in ionospheric research to overcome limitations of observations and models, and is an active area of research and development.

Some of the most comprehensive operational physics-based ionospheric data assimilation systems have been developed by Utah State University (e.g., Schunk et al., 2005; Scherliess et al., 2006) and the University of Southern California and Jet Propulsion Laboratory (e.g., Wang et al., 2004; Pi et al., 2009; Komjathy et al., 2010). Lee et al. (2012) recently assimilated the retrieved FORMOSAT-3/COSMIC

(F3/C) electron density profiles into a general circulation model of the thermosphere and ionosphere. Extensive variational data assimilation procedures have been developed with an empirical ionospheric model (e.g., Bust et al., 2004, 2007). Nicolls et al. (2009) applied this methodology to improve the E-region electron density retrieval from the F3/C data. Yue et al. (2011a, 2012) have assimilated F3/C and other radio occultation (RO) data into an empirical ionospheric model to obtain an improved global specification of the ionosphere.

The NOAA United States Total Electron Content (US-TEC) model (Fuller-Rowell et al., 2006) is designed to specify TEC over the continental United States (CONUS) from ground-based GPS slant TEC data. US-TEC uses the empirical ionosphere model, International Reference Ionosphere 95 (IRI95) (Bilitza, 1997), as a background model, and uses the empirical orthogonal functions (EOFs) and their coefficients (Spencer et al., 2004) to represent states in the Kalman filter (Kalman, 1960; Kalman and Bucy, 1961). The average rms (root mean square) error of US-TEC is 2.4 TEC units (Araujo-Pradere et al., 2007). The Kalman filter is one of the most commonly used approaches to ionospheric data assimilation. The Kalman filter update equation is given as

$$\boldsymbol{x}_\mathrm{a} = \boldsymbol{x}_\mathrm{b} + \mathbf{K}(\boldsymbol{y} - \mathbf{H}\boldsymbol{x}_\mathrm{b}), \tag{1}$$

$$\mathbf{K} = \frac{\mathbf{P}\mathbf{H}^T}{\mathbf{H}\mathbf{P}\mathbf{H}^T + \mathbf{R}}, \tag{2}$$

where $\boldsymbol{x}_\mathrm{a}$ is the state vector after an update, $\boldsymbol{x}_\mathrm{b}$ is the state vector of the background model, $\boldsymbol{y}$ is a vector of observations, $\mathbf{H}$ relates the state to the observations, $\mathbf{H}^T$ is transpose matrix of $\mathbf{H}$, $\mathbf{P}$ is the background model error covariance, $\mathbf{R}$ is the observation error covariance, and $\mathbf{K}$ is the Kalman gain (e.g., Welch and Bishop, 2000). In US-TEC, the Kalman filter state $\boldsymbol{x}_\mathrm{b}$ is composed of the coefficients of EOFs that characterize the principal modes of electron density vertical profiles. If Ψ_v and $\boldsymbol{a}_\mathrm{v}$ represent vertical EOFs and their coefficients, the electron density at a given altitude location v and longitude/latitude location h is expressed as $N_\mathrm{e}(v,h) = \sum_{m=1}^{6} \boldsymbol{a}_{\mathrm{v}_m}(h)\Psi_{\mathrm{v}_m}(v)$, where N_e is the grid-point electron density itself and m is an order of EOF. $\boldsymbol{x}$ in Eq. (1) is given by a vector of $\boldsymbol{a}_\mathrm{v}$ in US-TEC. The six EOFs are computed by using singular value decomposition; EOF1 is the dominant term of EOFs to represent the mean ionospheric profile. The higher-order EOFs gradually decrease their significance for allowing the reconstructed profile to depart from the mean (Spencer et al., 2004).

Mariner 4 first applied the RO observation technique to observe the Mars atmosphere and ionosphere in 1965 (Kliore et al., 1965). MicroLab-1 GPS/MET was launched in 1995 and applied to monitor the Earth's atmosphere and ionosphere by using the GPS RO technique (Hajj and Romans, 1998; Kursinski et al., 1997). The integrated content of ionospheric electron density, namely total electron content (TEC), has been measured between the GPS satellites and MicroLab-1. This is a way to observe the ionosphere horizontally at different altitudes and obtain the electron density profile using the Abel inversion technique. The F3/C mission was launched in April 2006, and has six micro-satellites in the different orbital planes. The GPS radio occultation experiment (GOX) is one of the satellite mission objectives, and observes the ionosphere and atmosphere vertical structure by using the RO observation technique. RO observations, particularly from F3/C, have significantly improved our capability of monitoring the global ionosphere (Cheng et al., 2006; Schreiner et al., 2007).

The overarching goal of our study is to assimilate not only the ground-based GPS slant TEC data but also F3/C RO slant TEC data into US-TEC. However, the original scheme was designed for assimilation of slant TEC between ground-based stations and GPS satellites, and is not ideal for assimilation of the RO slant TEC data. New data assimilation approaches that can better accommodate the RO data need to be developed. To this end, our study attempts to make the scheme more flexible; thus the Kalman filter equations will now be solved with respect to the grid-point electron density values (i.e., $\boldsymbol{x}$ is given by a vector of grid-point electron density itself, $N_\mathrm{e}(v,h)$) so that more realistic characteristics of the background model error can be incorporated. A new type of the background model error covariance is derived from an ensemble of IRI model outputs by representing location-dependent vertical and horizontal correlations using EOFs. Its performance is compared with a case where a simple stationary (i.e., location-independent) correlation is used in the Kalman filter. It should be noted that this study primarily focuses on implementation of the Kalman filter update step. The Kalman filter forecast step is outside of the scope of this study.

We use observing simulation system experiments (OSSEs), designed to mimic realistic observing systems of the ground-based GPS, and F3/C RO data to assess the impact of different types of the background model error covariance and the quality of assimilation analyses. Assimilation results are further validated with Millstone Hill incoherent scatter radar (ISR) electron density data, and compared with the F3/C GOX electron density profiles retrieved by the Abel inversion technique. Assimilation analyses are also presented in the form of TEC maps during both the daytime and nighttime. The use of F3/C RO data in data assimilation procedures is shown to improve both the vertical and horizontal structure of the ionospheric electron density distribution. The model domain extends from -140 to -60° with 2° resolution in longitude, from 10 to 60° with 2° resolution in latitude, and from 80 to 1000 km with 15 km resolution in altitude.

2 Data error and data thinning

When ground-based GPS and F3/C RO observation data are ingested into the data assimilation model, the observational errors need to be taken into account. Data from 200 ground-based GPS stations on the CONUS and F3/C RO slant TEC are used in examples shown later. More than 2000 GPS stations exist on the ground all over the world, and can yield the high-resolution TEC observations to determine horizontal structures of the ionosphere for monitoring various ionospheric phenomena and diurnal variations (Liu et al., 1996). However, most stations do not provide the differential code bias (DCB) of GPS receivers. Kakinami et al. (2009) used the Global Ionospheric Map (GIM) developed by the Jet Propulsion Laboratory (Mannucci et al., 1998) as a reference to eliminate the instrumental biases. The differential instrumental biases of GPS receivers are estimated by the GIM minimum TEC value during 04:00 and 06:00 local time at GPS receivers, while the DCB of GPS satellite is calibrated by using the Center for Orbit Determination in Europe (CODE) values (Schaer, 1999). The ground-based GPS slant TEC in this study is treated as DCB-free TEC after these DCB calibration processes. For space-based RO, the main error sources of the absolute TEC value obtained from RO include multipath effects, DCBs from GPS and low Earth orbit (LEO) satellites, and errors in leveling of the phase to the pseudorange TEC (Yue et al., 2011b). This study uses the F3/C podTec data produced by the COSMIC Data Analysis and Archival Center (CDAAC), and assumes that the absolute TEC values are free of DCB and multipath errors because these major errors are eliminated by CDAAC. In ground-based GPS observations with elevation angles of 20° or greater, the rms errors of the multipath effect on the phase are typically less than 1 mm (Bevis et al., 1992), which is insignificant; however those on the pseudorange are often in excess of 50 cm (Mannucci et al., 1998), which cannot be ignored.

Every GPS satellite can transmit signals at dual-frequency carrier phases (L1: 1575.42 MHz; L2: 1227.60 MHz). Coarse/acquisition (C/A: 1.023 MHz) and precision codes (P1: 10.23 MHz) are coded on the L1 carrier phase, and another precision code (P2: 10.23 MHz) is coded on the L2 carrier phase. The absolute and relative TEC can be calculated from the pseudorange and carrier phase, respectively (Sardón et al., 1994; Liu et al., 1996). Since the satellite and ground-based receivers error sources influence the precision of TEC calculated from pseudorange ($\mathrm{TEC_P}$), the precision of $\mathrm{TEC_P}$ is much lower than the TEC calculated from carrier phase ($\mathrm{TEC_L}$). The leveled TEC is obtained by leveling the carrier phase TEC to the pseudorange TEC to benefit from the precision of $\mathrm{TEC_L}$ and the accuracy of $\mathrm{TEC_P}$. The leveling error formula of each GPS observation arc is given by $\frac{\sqrt{\sum_{i=1}^{n}(\mathrm{TEC_{L}}_i - \mathrm{TEC_{P}}_i)^2}}{n}$ (Yue et al., 2011b), where n is the number of observations in each GPS arc and i is the ith observation data point in each GPS arc, where the cycle slip has been resolved. Thus, the leveling error of ground-based GPS data is influenced by the pseudorange multipath error and some unknown errors, which is difficultly estimated. Nevertheless, the leveling error of F3/C RO and ground-based GPS data would be taken into consideration when modeling the observation error covariance.

Data thinning is required because sampling space and time frequency of the GPS technique is significantly higher than the temporal and spatial resolution of data assimilation analysis. In this study, the grid-point resolution is 2° for longitude and latitude, and 15 km for altitude. To thin the data, 1 out of 31 continuous observation data points for a given GPS arc is selected for ingestion into the assimilation model. The original data rates of ground-based GPS and F3/C RO are 30 and 1 s, respectively. After data thinning, the data rates of ground-based GPS and F3/C RO are 15.5 min and 31 s, respectively. This number for the data thinning is determined by trial and error. The standard deviation from 31 continuous samples is calculated to determine the representativeness error resulting from the fact that scales resolved by the data assimilation model are lower than what is observed.

The main sources of GPS data errors have been described in above. Errors resulting from the DCB of GPS satellites, F3/C satellites, and ground-based GPS stations have been reduced before ingestion through the various calibration processes mentioned above. The leveling TEC error and representativeness error are the two types of errors that are combined to model the observation error covariance.

3 Covariance models

We develop two types of the background model error covariance in this study (**P** in Eq. 2): location-independent covariance and location-dependent covariance, and compare their effects on the quality of assimilation analysis. Location-independent (i.e., stationary) covariance refers to a covariance whose correlation structure is homogeneous and isotropic (in other words, the vertical and horizontal correlations at every grid location are identical). A Gaussian function is used to describe the stationary correlation in examples shown later. The length scale of longitude and latitude is 3° and the length scale for altitude is 50 km. These length scales are determined by a number of length scale tests. The variance of the background model error covariance is calculated from 62 different IRI electron density distributions, the equivalent of 2 months' worth of data, obtained by using randomized values of IG (ionosphere global) index and sunspot number IRI input parameters centered at the actual value of IG index and sunspot number on the experiment date. Here, we conduct experiments with synthetic data and real observation on 5 February 2008 and 21 October 2008, respectively. The IG index affects the *Nm*F2 and sunspot number changes the *hm*F2; the IG index and sunspot number are specified

by the random values sampled from a uniform distribution bounded by the given maximum and minimum value. In reality, spatial correlation of the electron density varies with location (i.e., inhomogeneous) and direction (i.e., anisotropic) in the ionosphere. Assuming the same model error correlation is likely to result in unexpected errors when assimilating observations, particularly from satellites. This study will examine how important this can be for determining ionospheric electron density distribution.

Here, the location-dependent correlation is designed by separating it into two parts: the vertical correlation and the horizontal correlation, and by using the EOFs to represent these correlations. First, we compute EOFs from the 62 different IRI ionospheric electron density distributions, N_e, by using the singular value decomposition. This is the same ensemble of IRI outputs used for calculating the variance. The electron density profiles are decomposed to three EOFs and their coefficients at each longitude and latitude location as in Eq. (3):

$$N_e^{(k)}(v) = \sum_{m=1}^{3} \boldsymbol{a}_{v_m}^{(k)} \Psi_{v_m}(v), \tag{3}$$

where $N_e^{(k)}$ is kth sample of the IRI electron density profiles ($k = 1, \ldots, 62$), v is the given altitude location, Ψ_v is a matrix that contains the EOFs for the vertical direction, and $\boldsymbol{a}_v$ is a vector of the vertical EOF coefficients. After determining the EOFs at each longitude and latitude location, the covariance of the EOF coefficients is computed from 62 sets, and then multiplied by the EOFs as in Eq. (4) to obtain the vertical covariance function $\mathbf{C}_v$:

$$\mathbf{C}_v = \Psi_v \mathrm{cov}(\boldsymbol{a}_v, \boldsymbol{a}_v^T) \Psi_v^T, \tag{4}$$

where cov denotes the covariance, and $\boldsymbol{a}_v^T$ and Ψ_v^T are the transpose of $\boldsymbol{a}_v$ and Ψ_v. The vertical correlation $\mathbf{Corr}_v$ can then be obtained after normalization and localization as in Eq. (5):

$$\mathbf{Corr}_{v_{i,j}} = \left(\frac{\mathbf{C}_{v_{i,j}}}{\sqrt{\mathbf{C}_{v_{i,j}}} \sqrt{\mathbf{C}_{v_{i,j}}}} \right) \circ \xi_{i,j} \tag{5}$$

where i and j are the element indices in the covariance matrix, ξ is the localization (i.e., tapering) function, and $\circ$ refers to an operation for the element by element multiplication. Localization is used to ameliorate effects of spurious correlations due to sampling errors. The Gaspari and Cohn function (Gaspari and Cohn, 1999) is used for the localization.

Figure 1a shows the vertical EOFs at a given longitude and latitude location. The location-independent vertical correlation (Fig. 1b) illustrates that the correlation is identical at every altitude, as calculated by using the same Gaussian function, while the location-dependent vertical correlation (Fig. 1c) shows that the vertical correlation is different at different altitudes. The vertical correlation at low altitude

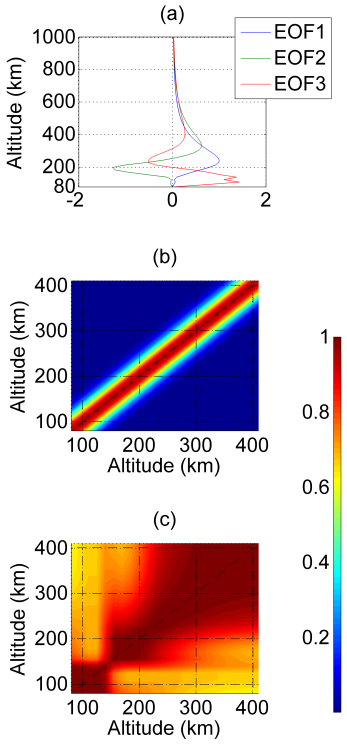

Figure 1. The vertical correlation at long −122° and lat 28°. **(a)** The EOFs calculated from 62 IRI N_e profiles with different sunspot numbers and IG indexes. **(b)** The location-independent vertical correlation modeled with a Gaussian function. **(c)** The location-dependent vertical correlation obtained from EOFs and its coefficients.

(below 150 km) is higher with lower-altitude locations but lower with higher-altitude locations. The vertical correlation at high altitude (above 150 km) is, on the other hand, higher with higher-altitude locations but lower with lower altitudes. This result suggests that the vertical correlation is strongly dependent on altitude locations. Since the vertical correlation is determined from the IRI empirical model outputs, rather than real observations, the vertical correlation used here is not free of errors when assimilating the real data. The length scale of localization function for altitude changes at different altitudes to reflect the vertical correlation length scale, which varies considerably with altitude.

The idea of calculating the horizontal correlation, the second part of location-dependent correlation, is similar to the vertical correlation. The kth horizontal map of IRI electron density at a given altitude, v, is decomposed to three EOFs and its coefficients as shown by Eq. (6).

$$N_e^{(k)}(h) = \sum_{m=1}^{3} \boldsymbol{a}_{h_m}^{(k)} \Psi_{h_m}(h), \tag{6}$$

where h is the given horizontal (longitude and latitude) location, Ψ_h is a matrix of the EOFs for the electron density on horizontal surface, and $\boldsymbol{a}_h$ is a vector of the horizontal

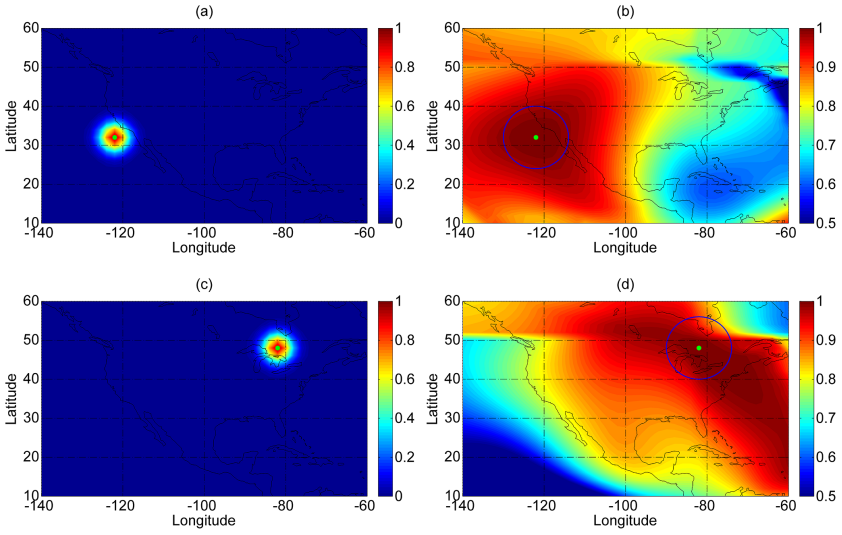

Figure 2. The horizontal correlation at 00:00 UTC. **(a)** The location-independent horizontal correlation modeled using a Gaussian function at altitude 200 km with respect to a grid point at long −122° and lat 32° marked by the green dot. **(b)** The location-dependent horizontal correlation modeled with the horizontal EOF profiles and its EOF coefficients' covariance for the same reference point as **(a)**. The blue circle surrounding the dot is the full length of the Gaspari and Cohn localization function, with which the correlation is tapered towards zero from the center (green dot) to the rim of the blue circle. **(c)** The location-independent horizontal correlation at altitude 200 km with respect to a point at long −82° and lat 48°. **(d)** The location-dependent horizontal correlation for the same reference point as **(c)**.

EOF coefficients. After decomposing the total of 62 maps into 3 EOFs and their coefficient, the covariance of the EOF coefficient is computed and then multiplied by the EOFs to convert it to the covariance of electron density on a grid, as in Eq. (7). The horizontal covariance $\mathbf{C}_\mathrm{h}$ is given by

$$\mathbf{C}_\mathrm{h} = \Psi_\mathrm{h}\mathrm{cov}(\boldsymbol{a}_\mathrm{h}, \boldsymbol{a}_\mathrm{h}^T)\Psi_\mathrm{h}^T, \tag{7}$$

where the $\boldsymbol{a}_\mathrm{h}^T$ and Ψ_h^T are the transpose matrixes of $\boldsymbol{a}_\mathrm{h}$ and Ψ_h.

The horizontal correlation is obtained after normalization and localization as in Eq. (8); this step is the same as calculating the vertical correlation.

$$\mathbf{Corr}_{\mathrm{h}_{i,j}} = \left(\frac{\mathbf{C}_{\mathrm{h}_{i,j}}}{\sqrt{\mathbf{C}_{\mathrm{h}_{i,j}}}\sqrt{\mathbf{C}_{\mathrm{h}_{i,j}}}}\right) \circ \xi_{i,j} \tag{8}$$

The length scale of localization for longitude and latitude is 3°. Figure 2a and b display the location-independent and dependent horizontal correlations at long −122°, lat 32°, and Fig. 2c and d display the location-independent and dependent horizontal correlations at another location, long −82°, lat 48°. As suggested by the fact that the horizontal correlation obtained from IRI empirical model outputs vary with location significantly, the location-dependent correlation information needs to be accounted for in the data assimilation scheme to successfully assimilate the real observations. As indicated by the blue circle in Fig. 2b and d, the extent of horizontal correlation is localized by the Gaspari and Cohn function to minimize the effect of spurious correlations resulting from the sampling error. Note that the correlation between the green point and surrounding locations outside of the blue circle is enforced to be zero. The location-dependent type of the background model error covariance is modeled by multiplying the location-dependent vertical correlation, location-dependent horizontal correlation, and model variance, as shown in Eq. (9).

$$\mathbf{P} = \mathbf{Var}_{i,j} \circ \mathbf{Corr}_{\mathrm{h}_{i,j}} \circ \mathbf{Corr}_{\mathrm{v}_{i,j}} \tag{9}$$

The advantage of modeling the background model error covariance in this manner is not only obtaining the variance but also the vertical and horizontal correlation of ionospheric electron density distribution varying according to its locations and geophysical conditions (e.g., day and night). The disadvantage is that it requires more computing time and memory than utilizing location-independent (i.e., stationary) correlation in the assimilation scheme. This issue can be dealt with by pre-computing the EOFs and the EOF coefficients covariance in advance and by adopting space matrix methods.

4 Assimilation experiments with synthetic data

The OSSEs, in which synthetically generated observations sampled from the IRI model output (i.e., the simulation truth) are assimilated, provide the assessment of the data assimilation (DA) procedure under idealistic conditions. A total of six different OSSEs have been conducted to examine the effects of different types of background model error covariance on the assimilation analysis quality. The simulation results are shown for the North American continent at 00:00 UTC on

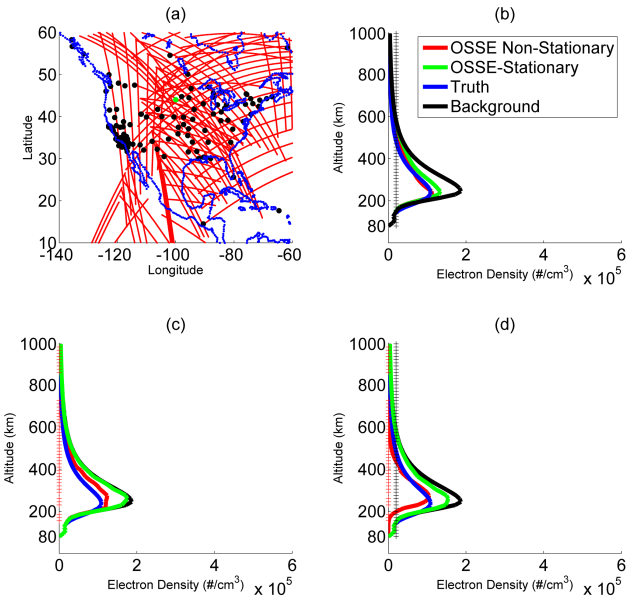

Figure 3. The OSSE result of the data assimilation model for 00:00 UTC on 5 February 2008. **(a)** The F3/C RO slant TEC paths of assimilated observations are shown as the red line, the black points are the ground-based GPS stations used in the OSSE. The data are accumulated over 1 h. The green dot indicates a location where electron density profiles are sampled for comparison and validation. **(b)** The electron density profiles are sampled from OSSE DA results obtained by assimilating the synthetic ground-based GPS data, which is integrated from the OSSE truth with different covariance models. The red line indicates the OSSE DA result with a location-dependent model error covariance (computed from EOFs), the green line is the OSSE DA result with a location-independent model error covariance (Gaussian), the blue line is the OSSE truth, and the black line is the background model. **(c)** The same as **(b)** but OSSE DA results are obtained by assimilating the synthetic F3/C data. **(d)** The same as **(b)** but OSSE DA results assimilated the synthetic data obtained from ground-based GPS and F3/C data. Note: the marks on the y axis indicate altitudes where slant TEC paths pass through this validation location, where red is used for F3/C and black is for ground-based GPS data.

5 February 2008 (Fig. 3). Note that the simulation truth and the background model states are different in the OSSEs presented here. The simulation truth is calculated from IRI with the lower IG index rather than the real IG index. This parameter setting makes synthetically generated observations of electron density lower than the climatological prediction by IRI in an effort to account for the tendency of IRI to overestimate the TEC during the extreme solar minimum conditions. This makes the simulation truth different from the background state. Two different kinds of slant TEC data are considered in the OSSEs: ground-based GPS data and F3/C occultation data.

Figure 3a displays the distributions of observations used in these experiments: ground-based GPS station (black point) and F3/C RO slant TEC path (red line). Six different experiment settings are as follows: (1) location-independent background model error covariance with synthetic ground-based GPS data (Fig. 3b), (2) location-independent background model error covariance with synthetic F3/C RO data (Fig. 3c), (3) location-independent background model error covariance with both ground-based and F3/C RO data (Fig. 3d), (4) location-dependent background model error covariance with synthetic ground-based GPS data (Fig. 3b), (5) location-dependent background model error covariance with synthetic F3/C RO data (Fig. 3c), and (6) location-dependent background model error covariance with both ground-based and F3/C RO data (Fig. 3d). The OSSE results are shown at long $-100°$ and at lat 44° to compare the vertical structures of assimilation analyses. Figure 3b and c compare electron density profiles from the IRI background model, the simulation truth, and data assimilation results for ground-based GPS data and F3/C RO data, respectively. The comparison suggests that assimilation results obtained using location-independent and location-dependent background model error covariance are both close to the simulation truth when assimilating ground-based GPS data. For assimilation of the F3/C RO data, on the other hand, a choice of the background model error covariance type makes a considerable difference. The electron density profile obtained using the location-independent covariance lies significantly away from the simulation truth and almost next to the background electron density. Figure 3d illustrates the OSSE electron density profile results for assimilation of both ground-based GPS data and F3/C RO data. The updated electron density profile using the location-dependent background model error covariance compares with the simulation truth far better than the one using location-independent model error covariance. The OSSE results suggest that the location-dependent background model error covariance effectively facilitates the assimilation of ground-based GPS and F3/C RO data independently, and of both simultaneously. In assimilation examples shown in the following sections, the location-dependent background model error covariance is used.

5 Assimilation results: TEC maps

We have conducted several data assimilation experiments over the CONUS with real ground-based GPS and F3/C RO slant TEC data on 21 October 2008. Assimilation results are presented as TEC, which is the column-integrated electron density from 80 to 1000 km. Results are compared to the background model TEC to examine the impact of F3/C RO data as well as ground-based GPS data. Figures 4 and 5 show TEC maps for the daytime (14:00–21:00 UTC) and nighttime (02:00–09:00 UTC) on 21 October 2008. At each hour UTC, three TEC maps are shown: a DA TEC map using

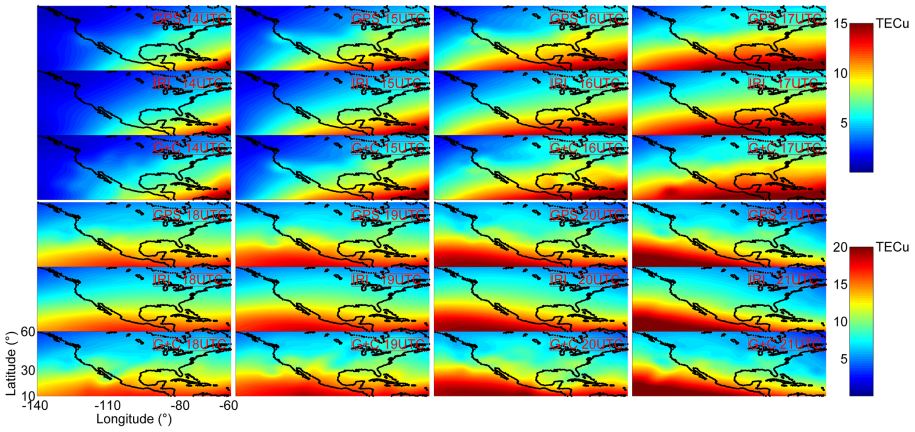

Figure 4. The DA and background model IRI TEC map of the North American Continent at daytime (14:00 to 17:00 UTC, top three rows) and 18:00 to 21:00 UTC (bottom three rows). Each time period has three different TEC maps, including a DA TEC map using ground-based GPS data, an IRI TEC map, and a DA TEC map using ground-based GPS and F3/C RO data.

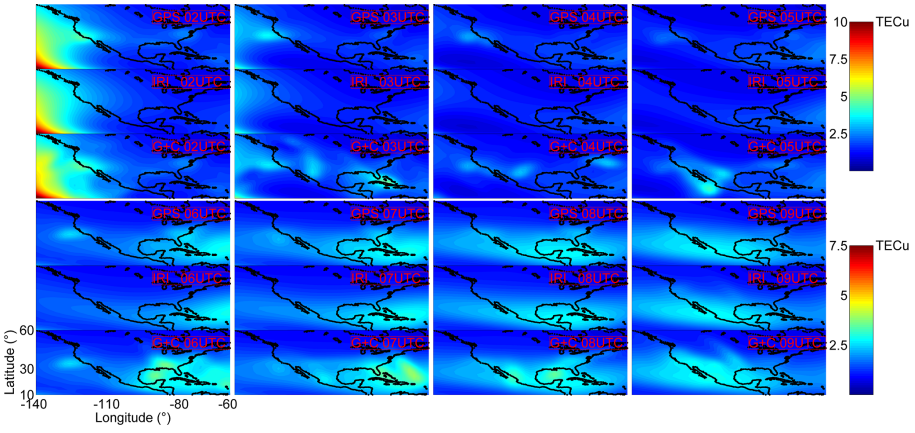

Figure 5. The DA and background model IRI TEC map of the North American Continent at nighttime (02:00 to 05:00 UTC, top three rows) and 06:00 to 09:00 UTC (bottom three rows). Each time period has three different TEC maps, including a DA TEC map using ground-based GPS data, an IRI TEC map, and a DA TEC map using ground-based GPS and F3/C RO data.

ground-based GPS data, an IRI background TEC map, and a DA TEC map using both ground-based GPS and F3/C RO data. It is clear that both types of data can modify the climatological TEC distribution predicted by the IRI successfully. Through comparison of two DA TEC maps, the influence of F3/C RO data is evident, particularly over the ocean, where ground-based GPS stations are absent. For instance, see the TEC maps at 02:00 UTC in Fig. 5, in which TEC have been updated over the ocean thanks to F3/C RO data. Our data assimilation system can effectively assimilate both space-based and ground-based GPS observations in the daytime and nighttime.

6 Validation with ISR data

The use of the location-dependent background model error covariance in the data assimilation scheme is essential when assimilating both ground-based GPS and F3/C RO data as suggested by the OSSE experiments. The accuracy of the data assimilation model must now be validated in terms of the model's ability to assimilate the real observation data. Here, the Millstone Hill incoherent scatter radar data are used to validate electron density profiles obtained from the assimilation of real ground-based GPS and F3/C RO data. Figure 6 displays the profiles at each 15 min interval between 16:00 and 17:45 UTC on 21 October 2008. Shown are the background model IRI (black), the data assimilation result (red is the DA electron density located at Millstone Hill; the green line is the DA electron density assimilating only ground-based GPS data), and the Millstone Hill data and related error bar (blue). The data assimilation results are obtained every 15 min. The displayed incoherent scatter radar profile is the median value over 15 min. There are three F3/C RO observation events over the region during this period. The alti-

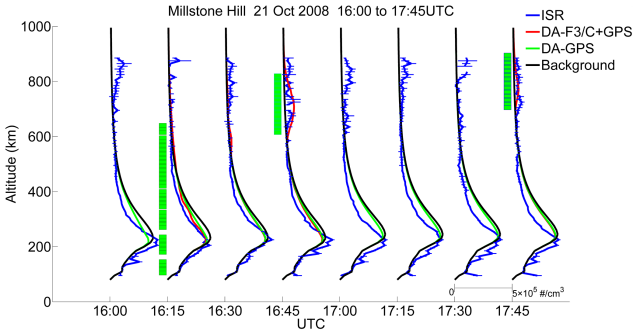

Figure 6. Comparison of data assimilation results and Millstone Hill incoherent scatter radar observations from 16:00 to 17:45 UTC, with a time period of 15 min. The red line is the DA electron density located at Millstone Hill and the green line is the DA electron density assimilating only ground-based GPS data, while the black line is the background of the DA model. The blue line is the observation and error bars of Millstone Hill incoherent scatter radar. The green boxes indicate that the altitude had F3/C RO passing through.

tude grids where F3/C RO paths intersect with the ISR line of sight are indicated by green boxes at 16:15, 16:45, and 17:45 UTC. The F3/C RO paths pass through at different altitude regions over Millstone Hill over this period; they pass through the *E* region and *F* region at 16:15 UTC, and between 500 and 800 km altitude at 16:45 and 17:45 UTC. In these three time periods the data assimilation result agrees well with ISR electron density; the rms deviation between DA results and ISR data is $4.06 \times 10^4 \,\#\,\mathrm{cm}^{-3}$. When no F3/C RO data are assimilated in addition to ground-based GPS data, the agreement of DA and ISR electron density profiles is considerably poorer; the rms deviation between DA results and ISR data is $4.72 \times 10^4 \,\#\,\mathrm{cm}^{-3}$.

The F3/C electron density profile calculated from the Abel inversion (obtained from CDAAC) can also be compared to our data assimilation analysis. The comparison is presented for 16:15 UTC on 21 October 2008, when the RO path is located close to Millstone Hill. Figure 7a displays the 3-D observing geometry of Millstone Hill ISR (blue) and F3/C RO (red), and the TEC map from the DA result is shown on the longitude–latitude plane at the bottom. Since the ISR location and F3/C RO tangent point location are different, we validated our DA result with ISR and F3/C RO electron density separately. Figure 7b compares vertical electron density profiles from the ISR and data assimilation analysis at the Millstone Hill location. The ISR error bar plotted along the ISR profile suggests high measurement uncertainty in the upper portion of the profile. The data assimilation electron density profile agrees well with ISR from altitude 200 to 400 km, where the ISR error is relatively small, including *hm*F2 and *Nm*F2 values. Figure 7c compares the Abel inversion retrieval of electron density profile (black) with the data assimilation result (red) along the RO tangent point (i.e., red line in Fig. 7a). The *hm*F2 from data assimilation results is

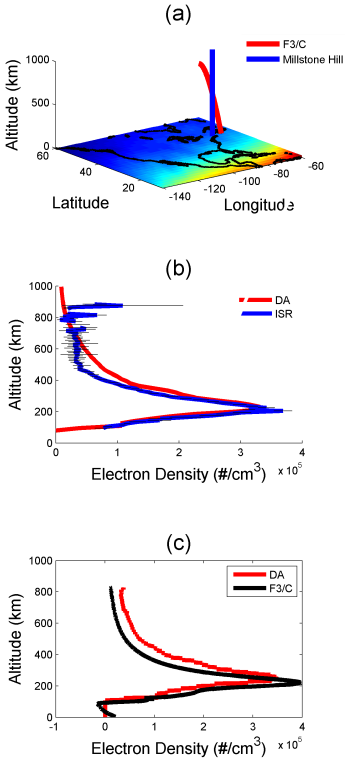

Figure 7. The comparison of the data assimilation results, Millstone Hill incoherent scatter radar observation, and F3/C electron density profile from the Abel inversion. **(a)** The location of F3/C RO tangent point electron density profile (red) and the location of Millstone Hill observation electron density profile (blue). **(b)** The electron density profile of DA (red), ISR (blue), and ISR's error bars (black) over Millstone Hill. **(c)** The electron density profile of DA (red) and F3/C (black) along the RO tangent point.

estimated to be slightly higher than the Abel inversion result, while the *Nm*F2 is estimated to be lower.

7 Discussion

In this study, we develop a new background model error covariance model to account for spatially variable correlation patterns of the model errors. Even though the location-dependent covariance model reflects more realistic correlations, the OSSE results indicate that both location-independent and location-dependent covariance work equally well for assimilation of ground-based GPS data. (See Fig. 3b, where electron density profiles obtained by using both types of the covariance models are shown to produce similar results and compare well with the simulation truth.) This result suggests that the vertical and horizontal error correlation might not have significant importance when assimilating the ground-based GPS slant TEC. Since the radio signal is transmitted from GPS satellites to ground-based receivers, the ground-based GPS slant TEC data tend to con-

tain more information about the horizontal ionospheric structure and less about the vertical ionospheric structure. Vertical correlation in the background model error covariance is rather irrelevant in inverting the ground-based GPS slant TEC data since they are a nearly vertically integrated quantity. Moreover, the horizontal extent of ground-based GPS observations is mostly limited in the vicinity of ground-based stations, and therefore the long-range horizontal correlation does not play a significant role either.

RO slant TEC values are computed from radio signals transmitted from GPS satellites to LEO satellites that pass through the ionosphere at different altitudes over extensively large horizontal areas, and F3/C RO data can thus provide vertically resolved ionospheric information. To invert RO slant TEC data accurately, the vertical and horizontal correlation in the background model error covariance needs to be realistic. The OSSE results presented in Fig. 3c demonstrate this point, showing that electron density profiles obtained using a more realistic covariance model are closer to the simulation truth. When assimilating the F3/C RO data, it is therefore important that the background model error covariance reflects realistic location-dependent correlation structures.

The accuracy of the background model error covariance affects the quality of data assimilation analyses, especially when assimilating different kinds of GPS data. The OSSE results shown in Fig. 3d, obtained from assimilation of ground-based and RO synthetic data, illustrate this point clearly. Electron density profiles estimated by using the location-dependent error covariance are closer to the simulation truth in comparison to the cases with the location-independent error covariance. Even though the OSSE electron density profiles obtained by using the location-independent error covariance is reasonable for assimilating ground-based GPS data alone, the results are deteriorated when assimilating the same data in addition to the RO data. These detailed comparisons suggest that the choice of the background model error covariance needs to be suitable for all types of GPS data being assimilated; otherwise the accuracy of data assimilation analysis would not be optimal.

It should be noted that the current study has not considered the Kalman filter forecast step, so our approach is closer to the optimal interpolation for the moment. In the Kalman filter, the background model error covariance is expected to evolve and become more realistic over time through a recursive application of update and forecast steps in theory. In reality, it is difficult to fully incorporate nonlinear ionospheric dynamics into the Kalman filter forecast step. The model dynamics are often simplified, and the evolution of background (forecast) model error covariance is therefore approximated. The current study represents a low-dimensional modeling of the background model error covariance, which can facilitate the future implementation of the Kalman filter in the global domain. This point will be demonstrated in our future work. As part of our future work, the Taiwan Ionospheric Model (TWIM), which is constructed from F3/C RO electron density profiles (Tsai et al., 2009), can be used in the place of the IRI model in our data assimilation study to increase the accuracy of background model vertical structure.

To validate the electron density profiles, the DA results are evaluated and compared to the Millstone Hill ISR data from 16:00 to 17:45 UTC at every 15 min interval on 21 October 2008. Both ground-based GPS and F3/C observations are located closed to the ISR at three intervals: 16:15, 16:45, and 17:45 UTC. In these three time periods, the rms deviation between ISR data and DA results obtained from assimilation of RO and ground-based GPS data is $4.06 \times 10^4 \,\#\,\mathrm{cm}^{-3}$. At other time intervals, only ground-based GPS data are available. DA results agree poorly with ISR data when only ground-based GPS data are assimilated. The rms deviation between ISR data and DA results obtained from assimilation of only ground-based GPS data is $4.72 \times 10^4 \,\#\,\mathrm{cm}^{-3}$. Since the ground-based GPS data contain little information about the vertical ionospheric structure, assimilating ground-based GPS data alone will not modify the vertical structure predicted by the background model. On the other hand, the results from assimilation of both ground-based GPS and F3/C RO slant TEC agree better with the ISR electron density profile in the F region at (16:15 UTC) and at high altitude from 500 to 800 km (16:45 and 17:45 UTC). The validation with the ISR data supports our premise that our data assimilation procedure with the location-dependent background model error covariance effectively reconstructs the 3-D electron density from both ground-based GPS and F3/C RO data.

The tangent points of the F3/C are aligned with the Millstone Hill ISR line of sight at 16:15 UTC on 21 October 2008, when the DA results compare well with the ISR electron density profile. The comparison of our DA results with the ISR electron density profile and with the profile retrieved from the F3/C using the Abel inversion is shown in Fig. 7b and c, respectively. This comparison reflects the respective observing geometry of ISR and F3/C RO techniques, since the later one is slightly veered from vertical. The DA electron density profile agrees well with the ISR data from altitude 200 to 400 km, where the ISR error is relatively small, including *hm*F2 and *Nm*F2 values. In comparison with the Abel inversion result, the *hm*F2 is estimated to be slightly higher, while the *Nm*F2 is estimated to be lower. Below altitude 150 km, the Abel inversion yields unphysical negative electron density value. Liu et al. (2010) have shown that electron density profiles obtained by the Abel inversion are prone to a large amount of error below about 200 km. With the help of regularization through the background model error covariance in the Kalman filter, electron density profiles resulting from our data assimilation procedure are more robust than the Abel inversion results.

The ground-based GPS technique can provide valuable continual monitoring of the ionosphere, but its spatial coverage is regional. To achieve global monitoring of the ionosphere, including the oceans and remote regions where it is difficult to deploy ground-based stations, space-based ob-

serving techniques like the F3/C are crucial. TEC maps, shown in Figs. 4 and 5 for both daytime and nighttime, demonstrate this point. Because of its spatially limited observing geometry, the ground-based GPS observation can modify the background ionosphere horizontal structure only in the vicinity of station locations. On the other hand, the space-based GPS technique can provide greater spatial coverage because RO paths pass through the ionosphere rather horizontally. Data assimilation approaches, such as the one presented here, can take advantage of both observing techniques to improve the global ionospheric specification.

In addition, the TEC maps display the feature akin to the plasmaspheric tail (ionospheric plume) at 20:00 UTC (Fig. 4) (Foster et al., 2002). The similar plasmaspheric tail signature is shown in both assimilation results but is not seen in the background model. Our data assimilation procedure has the capability to reconstruct realistic transient ionospheric features, such as plasmaspheric tails, that are absent in IRI. Resulting assimilation analyses can be used for storm time studies to identify the plasmaspheric foot points in the ionosphere.

8 Conclusions

In this study, we presented a new approach to assimilate F3/C RO data as well as ground-based GPS data into the background model IRI and examined the impact of RO data on the reconstructed 3-D ionospheric election density structure. Unlike the current US-TEC model, which solves Kalman filter equations with respect to EOF coefficients, we developed a new data assimilation procedure in which the Kalman filter equations are solved in terms of grid-point electron density in order to accommodate a more flexible regularization strategy. Four main conclusions were drawn from our results.

The first conclusion is, as illustrated by the OSSE experiment results, that the location-dependent model error covariance facilitated inverting both ground-based GPS and F3/C RO slant TEC data independently, and that it is a key to successfully assimilating both data at the same time. This conclusion was drawn from demonstrating the limitation of the location-independent covariance model (based on the Gaussian function) for the assimilation of RO observational data, and developing a new covariance model whose correlation structures depend on longitude, latitude, and altitude location. The location-dependent covariance model was constructed by representing vertical and horizontal correlations with EOFs and their coefficients as shown in Figs. 1 and 2. OSSE experiments with the location-independent model error covariance showed that results were satisfactory for ground-based GPS data assimilation, but the OSSE result assimilating F3/C RO slant TEC does not agree well with the simulation truth. Therefore, the OSSE result illustrated that the location-dependent model error covariance worked well with both datasets separately, and even better assimilating both simultaneously.

Second, we validated assimilation analyses using Millstone Hill ISR data and concluded that assimilation of ground-based and RO data using our new procedure improved the agreement with ISR electron density profiles. This was true particularly when F3/C RO data are present in the vicinity of Millstone Hill, since the DA scheme is able to correct altitude structures quite well.

The third conclusion is that our scheme can produce a more robust profile than the Abel inversion thanks to regularization through the use of more realistic background model error covariance in the Kalman filter update equation. This point was demonstrated by sampling our DA results along the RO tangent points, and comparing them with F3/C RO electron density profiles calculated from the Abel inversion, as shown in Fig. 7 for the Millstone Hill location. Our DA results are generally similar to the Abel inversion results, but, importantly, our scheme was able to produce more robust profiles due to an improved regularization in inversion methods.

Our final conclusion is that the F3/C RO could improve the electron density results over greater areas, including oceans and remote regions where no ground-based stations exist. Furthermore, the F3/C RO data have the potential to improve the altitude structures of DA analysis. For the F3/C mission, 1000–2500 RO events per day (3000 at maximum) have occurred; however the current RO global coverage is not complete at a given time. This should be greatly improved when FORMOSAT-7/COSMIC-2 (F7/C2), with 12 micro-satellites, is launched in 2016 and 2018. Each micro-satellite will be equipped with the appropriate satellite signal receiver to conduct the RO experiment with GNSS and GLONASS. This new mission is expected to yield more than 14 000 RO events per day. By assimilating F7/C2 RO data into our data assimilation model, the global ionosphere specification will be significantly improved. Our new DA procedure can also be incorporated into the NOAA/SWPC ionospheric assimilation model US-TEC to increase the assimilation analysis accuracy. With the expanded availability of RO data, the electron density distribution analysis will be improved over greater regions, including areas where ground-based GPS stations are absent, and the approach presented in this paper supports such future prospects.

Acknowledgements. Chi-Yen Lin sincerely thanks Karen Fay O'Loughlin for her helpful assistance with the paper. Support for this study is provided through NASA award NNX09AJ83G to the University of Colorado at Boulder, and the Taiwan National Science Council (NSC) grant NSC 102-2628-M-008-001. The authors gratefully acknowledge the International GNSS Service (IGS) for providing GPS data and COSMIC Data Analysis and Archival Center (CDAAC) and the Taiwan Analysis Center for COSMIC (TACC) for the FORMOSAT-3/COSMIC data. Radar observations at Millstone Hill are supported by a cooperative

agreement between the US National Science Foundation and the Massachusetts Institute of Technology.

Edited by: U. Foelsche

References

Araujo-Pradere, E. A., Fuller-Rowell, T. J., Spencer, P. S. J., and Minter, C. F.: Differential validation of the USTEC model, Radio Sci., 42, RS3016, doi:10.1029/2006RS003459, 2007.

Bevis, M., Businger, S., Herring, T., Rocken, C., Anthes, R., and Ware, R., GPS meteorology: Remote sensing of atmospheric water vapor using the Global Positioning System, J. Geophys. Res., 97, 15787–15801, 1992.

Bilitza, D.: International Reference Ionosphere – Status 1995/96, Adv. Space Res., 20, 1751–1754, 1997.

Bust, G. S., Garner, T. W., and Gaussiran II, T. L.: Ionospheric Data Assimilation Three-Dimensional (IDA3D): A global, multisensor, electron density specification algorithm, J. Geophys. Res., 109, A11312, doi:10.1029/2003JA010234, 2004.

Bust, G. S., Crowley, G., Garner, T. W., Gaussiran II, T. L., Meggs, R. W., Mitchell, C. N., Spencer, P. S. J., Yin, P., and Zapfe, B.: Four-dimensional GPS imaging of space weather storms, Space Weather, 5, S02003, doi:10.1029/2006SW000237, 2007.

Cheng, C. Z. F., Kuo, Y. H., Anthes, R. A., and Wu, L.: Satellite constellation monitors global and space weather, Eos T. Am. Geophys. Un., 87, 166, doi:10.1029/2006EO170003, 2006.

Foster, J. C., Coster, A. J., Erickson, P. J., Goldstein, J., and Rich, F. J.: Ionospheric signatures of plasmaspheric tails, Geophys. Res. Lett., 29, 1623, doi:10.1029/2002GL015067, 2002.

Fuller-Rowell, T., Araujo-Pradere, E., Minter, C., Codrescu, M., Spencer, P., Robertson, D., and Jacobson, A. R.: USTEC: A new data assimilation product from the Space Environment Center characterizing the ionospheric total electron content using real-time GPS data, Radio Sci., 41, RS6003, doi:10.1029/2005RS003393, 2006.

Gaspari, G. and Cohn, S. E.: Construction of correlation functions in two and three dimensions, Q. J. Roy. Meteor. Soc., 125, 723–757, doi:10.1002/qj.49712555417, 1999.

Hajj, G. A. and Romans, L. J.: Ionospheric electron density profiles obtained with the global positioning system: results from the GPS/MET experiment, Radio Sci., 33, 175–190, doi:10.1029/97RS03183, 1998.

Kakinami, Y., Chen, C. H., Liu, J. Y., Oyama, K.-I., Yang, W. H., and Abe, S.: Empirical models of Total Electron Content based on functional fitting over Taiwan during geomagnetic quiet condition, Ann. Geophys., 27, 3321–3333, doi:10.5194/angeo-27-3321-2009, 2009.

Kalman, R. E.: A new approach to linear filtering and prediction problems, J. Basic Eng., 82, 34–45, doi:10.1115/1.3662552, 1960.

Kalman, R. E. and Bucy, R.: New results in linear filtering and prediction theory, J. Basic Eng., 83, 95–108, doi:10.1115/1.3658902, 1961.

Kliore, A. J., Cain, D. L., Levy, G. S., Eshleman, V. R., Fjeldbo, G., and Drake, E. D.: Occultation experiment: Results of the first direct measurement of Mars' atmosphere and ionosphere, Science, 149, 1243–1248, doi:10.1126/science.149.3689.1243, 1965.

Komjathy, A., Wilson, B., Pi, X., Akopian, V., Dumett, M., Iijima, B., Verkhoglyadova, O., and Mannucci, A. J., JPL/USC GAIM: On the impact of using COSMIC and ground-based GPS measurements to estimate ionospheric parameters, J. Geophys. Res., 115, A02307, doi:10.1029/2009JA014420, 2010.

Kursinski, E. R., Hajj, G. A., Schofield, J. T., Linfield, R., and Hardy, K. R.: Observing Earth's atmosphere with radio occultation measurements using the Global Positioning System, J. Geophys. Res., 102, 23429–23465, doi:10.1029/97JD01569, 1997.

Lee, I. T., Matsuo, T., Richmond, A. D., Liu, J. Y., Wang, W., Lin, C. H., Anderson, J. L., and Chen, M. Q.: Assimilation of FORMOSAT-3/COSMIC electron density profiles into a coupled thermosphere/ionosphere model using ensemble Kalman filtering, J. Geophys. Res., 117, A10318, doi:10.1029/2012JA017700, 2012.

Liu, J. Y., Tsai, H. F., and Jung, T. K., Total electron content obtained by using the global positioning system, Terr. Atmos. Ocean. Sci., 7, 107–117, 1996.

Liu, J. Y., Lin, C. Y., Lin, C. H., Tsai, H. F., Solomon, S. C., Sun, Y. Y., Lee, I. T., Schreiner, W. S., and Kuo, Y. H.: Artificial plasma cave in the low-latitude ionosphere results from the radio occultation inversion of the FORMOSAT-3/COSMIC, J. Geophys. Res., 115, A07319, doi:10.1029/2009JA015079, 2010.

Mannucci, A. J., Wilson, B. D., Yuan, D. N., Ho, C. H., Lindqwister, U. J., and Runge, T. F.: A global mapping technique for GPS-derived ionospheric total electron content measurements, Radio Sci., 33, 565–582, doi:10.1029/97RS02707, 1998.

Nicolls, M. J., Rodrigues, F. S., Bust, G. S., and Chau, J. L.: Estimating E region density profiles from radio occultation measurements assisted by IDA4D, J. Geophys. Res., 114, A10316, doi:10.1029/2009JA014399, 2009.

Pi, X., Mannucci, A. J., Iijima, B. A., Wilson, B. D., Komjathy, A., Runge, T. F., and Akopian, V.: Assimilative modeling of ionospheric disturbances with FORMOSAT-3/COSMIC and ground-based GPS measurements, Terr. Atmos. Ocean. Sci., 20, 273–285, doi:10.3319/TAO.2008.01.04.01(F3C), 2009.

Sardón, E., Rius, A., and Zarraoa, N.: Estimation of the transmitter and receiver differential biased and the ionospheric total electron content from Global Positioning System Observations, Radio Sci., 29, 577–586, doi:10.1029/94RS00449, 1994.

Schaer, S.: Mapping and predicting the Earth's ionosphere using the Global Positioning System, Ph.D. dissertation, Astron. Inst., Univ. of Bern, Bern, 1999.

Scherliess, L., Schunk, R. W., Sojka, J. J., Thompson, D. C., and Zhu, L.: The USU GAIM Gauss-Markov Kalman filter model of the ionosphere: Model description and validation, J. Geophys. Res., 111, A11315, doi:10.1029/2006JA011712, 2006.

Schreiner, W., Rocken, C., Sokolovskiy, S., Syndergaard, S., and Hunt, D.: Estimates of the precision of GPS radio occultations from the COSMIC/FORMOSAT-3 mission, Geophys. Res. Lett., 34, L04808, doi:10.1029/2006GL027557, 2007.

Schunk, R. W., Scherliess, L., Sojka, J. J., Thompson, D., and Zhu, L.: Ionospheric weather forecasting on the horizon, Space Weather, 3, S08007, doi:10.1029/2004SW000138, 2005.

Spencer, P. S. J., Robertson, D. S., and Mader, G. L.: Ionospheric data assimilation methods for geodetic applications, paper presented at IEEE PLANS 2004, Inst. Electr. Electron. Eng., Monterey, Calif., 26–29 April, 2004.

Tsai, L. C., Liu, C. H., Hsiao, T. Y., and Huang, J. Y.: A near real-time phenomenological model of ionospheric electron density based on GPS radio occultation data, Radio Sci., 44, RS5002, doi:10.1029/2009RS004154, 2009.

Wang, C., Hajj, G., Pi, X., Rosen, I. G., and Wilson, B.: Development of the global assimilative ionospheric model, Radio Sci., 39, RS1S06, doi:10.1029/2002RS002854, 2004.

Welch, G. and Bishop, G.: An introduction to the Kalman filter, Dept. Comput. Sci., Univ. North Carolina, Chapel Hill, Tech. Rep. TR95041, 2000.

Yue, X., Schreiner, W. S., Lin, Y. C., Rocken, C., Kuo, Y. H., and Zhao, B.: Data assimilation retrieval of electron density profiles from radio occultation measurements, J. Geophys. Res., 116, A03317, doi:10.1029/2010JA015980, 2011a.

Yue, X., Schreiner, W. S., Hunt, D. C., Rocken, C., and Kuo, Y. H.: Quantitative evaluation of the low Earth orbit satellite based slant total electron content determination, Space Weather, 9, S09001, doi:10.1029/2011SW000687, 2011b.

Yue, X., Schreiner, W. S., Kuo, Y.-H., Hunt, D. C., Wang, W., Solomon, S. C., Burns, A. G., Bilitza, D., Liu, J.-Y., Wan, W., and Wickert, J.: Global 3-D ionospheric electron density reanalysis based on multisource data assimilation, J. Geophys. Res., 117, A09325, doi:10.1029/2012JA017968, 2012.